Results in Physics 6 (2016) 897–903

Contents lists available at ScienceDirect

Results in Physics

journal homepage: www.journals.elsevier.com/results-in-physics

Three-dimensional flow of nanofluid with Cattaneo–Christov double diffusion

Tasawar Hayat [a,b], Taseer Muhammad [a,*], Ahmed Alsaedi [b], Bashir Ahmad [b]

[a] Department of Mathematics, Quaid-I-Azam University, Islamabad 44000, Pakistan

[b] Nonlinear Analysis and Applied Mathematics (NAAM) Research Group, Department of Mathematics, Faculty of Science, King Abdulaziz University, Jeddah 21589, Saudi Arabia

ARTICLE INFO

Article history:
Received 3 October 2016
Received in revised form 24 October 2016
Accepted 25 October 2016
Available online 9 November 2016

Keywords:
Three-dimensional flow
Nanoparticles
Cattaneo–Christov double diffusion
Optimal homotopy analysis method (OHAM)

ABSTRACT

Three dimensional (3D) boundary-layer flow of viscous nanofluid has been investigated in the presence of Cattaneo–Christov double diffusion. A bi-directional linearly stretching sheet has been used to create the flow. Thermal and concentration diffusions are characterized by introducing Cattaneo–Christov fluxes. Novel attributes regarding Brownian motion and thermophoresis are retained. The conversion of nonlinear partial differential system to nonlinear ordinary differential system is done through suitable transformations. The resulting nonlinear systems are solved. Graphs have been sketched in order to investigate that how the temperature and concentration profiles are affected by distinct physical flow parameters. Further the skin friction and heat and mass transfer rates are numerically computed and discussed. Our findings depict that temperature and concentration distributions are decreasing functions of thermal and concentration relaxation parameters.

1. Introduction

The investigations on boundary-layer flows past a stretching surface are significantly enhanced during the past few decades due to their practical significance in industrial and technological processes. Such flows commonly involve in extrusion of plastic sheets, paper production, wire drawing, drawing of plastic films, hot rolling, glass fiber production and several others. Sakiadis [1] provided an analysis to examine the flow induced by a continuously moving plate. Then Crane [2] continued the work of Sakiadis [1] for stretching sheet and provided an exact solution for velocity field. After the innovative work of Crane, several researchers have investigated different problems of stretching surface. Most of the investigations in the literature deal with the two-dimensional flow past a stretching surface. There are scarce studies available in the literature regarding three-dimensional (3D) flow by a stretching surface. With this viewpoint, Wang [3] discussed three-dimensional (3D) flow induced by a stretching surface. He proved that classical problems of two dimensional (2D) and axisymmetric flows induced by stretching surface can be easily achieved from this study. Then Ariel [4] examined the three-dimensional flow by a stretching surface. He provided both exact and homotopy perturbation solutions of the governing system. Hydromagnetic unsteady three-dimensional flow over a stretching surface is reported by Xu et al. [5]. Unsteady MHD three-dimensional flow saturating porous space past a stretching surface is addressed by Hayat et al. [6]. Liu et al. [7]studied three-dimensional (3D) flow of viscous liquid by an exponentially stretching surface. Recently Hayat et al. [8]examined Soret and Dufour effects in three-dimensional (3D) flow of viscous liquid due to an exponentially stretching surface subject to porous medium, chemical reaction and heat source/sink.

The phenomenon of heat transfer happens if there exists difference in temperature between the bodies or between the components of the similar body. This phenomena has vast technological and industrial use, for example, in microelectronics, cooling of atomic reactors, fuel cells, power generation, pasteurization of food, energy production etc. The well-known law of heat conduction proposed by Fourier [9] is mostly used for heat transfer attributes from the time it showed up in the literature. Cattaneo [10] changed this law by including relaxation time. This term overcomes the "paradox of heat conduction". Christov [11] further changed the Cattaneo theory [10] by replacing the time derivative with Oldroyd upper-convected derivative. This theory is termed as Cattaneo–Christov heat flux theory. Straughan [12] employed heat flux model by Cattaneo–Christov expression to explore thermal convection in horizontal layer of Newtonian liquid. Ciarletta and Straughan [13] showed the structural stability and uniqueness of solutions for an energy equation with heat flux by

* Corresponding author.
E-mail address: taseer_qau@yahoo.com (T. Muhammad).

http://dx.doi.org/10.1016/j.rinp.2016.10.017
2211-3797/© 2016 Published by Elsevier B.V.

Cattaneo–Christov expression. Haddad [14] discussed the thermal instability in the Brinkman porous medium by employing heat flux with Cattaneo–Christov expression. Han et al. [15] addressed the stretched flow of Maxwell material through heat flux by Cattaneo–Christov expression. Mustafa [16] used heat flux through Cattaneo–Christov expression in order to explore heat transfer for flow of Maxwell material. He provided numeric and analytic solutions of governing flow systems. Khan et al. [17] provided a numerical analysis to study the thermal relaxation attributes in Maxwell liquid flow by an exponentially stretching surface. Hayat et al. [18] performed a comparative study for flows of viscoelastic materials by considering heat flux through Cattaneo–Christov expression. Li et al. [19] analyzed the magnetohydrodynamic slip flow of viscoelastic fluid past a vertical stretching surface with Cattaneo–Christov heat flux. Mushtaq et al. [20] numerically reported the Sakiadis flow of Maxwell fluid by considering heat flux through Cattaneo–Christov theory. Darcy–Forchheimer flow of an Oldroyd-B fluid with variable thermal conductivity and Cattaneo–Christov heat flux is examined by Shehzad et al. [21]. Recently Hayat et al. [22] studied the magnetohydrodynamic flow of an Oldroyd-B fluid with Cattaneo–Christov heat flux and homogeneous-heterogeneous reactions.

At present the nanotechnology is an interesting area of research due to its widespread scope of applications in the technological and engineering processes. The development of enhancing heat transfer techniques is the main concern of the recent scientists working in this field. The argument behind the fluid additives is to enhance the thermal performance of ordinary liquids like oil, water and ethylene–glycol mixture. Many researchers have reported the impact of solid–liquid mixture for heat transfer improvement. Various aspects like clogging, abrasion, additional pressure loss etc. have been pointed out which made such mixture inappropriate to enhance thermal performance. Choi [23] proposed the idea of nanofluid. He experimentally verified that the thermal performance of carrier-liquid enhance dramatically by submersion of tiny size solid or metallic particles. Buongiorno [24] has explored the mechanisms of nanofluid via moment of nanoparticles in ordinary base fluid. Such mechanisms include nanoparticles size, magnus effect, inertia, particle agglomeration, Brownian motion, thermophoresis and volume fraction. The recent attempts on flows of nanofluids can be seen in the investigations [25–50] and several studies therein.

Our inspiration in present attempt is covered by four novel aspects. Firstly to model and analyze the three dimensional (3D) flow of viscous nanoliquid induced by a stretching surface. Secondly to examine the heat and mass transfer attributes through the generalized Fourier's and Fick's laws, namely Cattaneo–Christov double diffusion expressions. Thirdly to employ the Buongiorno's model of nanofluids. Thermophoretic and Brownian motion aspects are considered. Fourth to derive convergent solutions for the velocities, temperature and concentration through optimal homotopy analysis method (OHAM) [51–60]. The contributions of various pertinent parameters are studied and discussed. Further skin friction and heat and mass transfer rates at the surface are also analyzed through numerical values.

2. Formulation

We intend to elaborate the three dimensional (3D) flow of viscous nanoliquid over a linear stretching sheet with constant surface temperature and concentration. The Brownian motion and thermophoresis aspects are taken into consideration. Here x- and y-axes are along the stretching surface while z-axis is normal to the sheet. Let $U_w(x) = ax$ and $V_w(y) = by$ be the stretching velocities along the x- and y-directions respectively. The heat and mass transfer mechanisms are examined through Cattaneo–Christov double diffusion expressions. Resulting equations of mass, momentum, energy and concentration for boundary layer considerations are

$$\frac{\partial u}{\partial x}+\frac{\partial v}{\partial y}+\frac{\partial w}{\partial z}=0, \tag{1}$$

$$u\frac{\partial u}{\partial x}+v\frac{\partial u}{\partial y}+w\frac{\partial u}{\partial z}=\nu\frac{\partial^2 u}{\partial z^2}, \tag{2}$$

$$u\frac{\partial v}{\partial x}+v\frac{\partial v}{\partial y}+w\frac{\partial v}{\partial z}=\nu\frac{\partial^2 v}{\partial z^2}. \tag{3}$$

Note that u, v and w represent the components of velocity in x-, y- and z-directions respectively while $\nu(=\mu/\rho_f), \mu$ and ρ_f denote kinematic viscosity, dynamic viscosity and density of base liquid respectively. The Cattaneo–Christov double diffusion theory has been introduced in characterizing thermal and concentration diffusions with heat and mass fluxes relaxations respectively. Then the frame indifferent generalization regarding Fourier's and Fick's laws (which is named as Cattaneo–Christov anomalous diffusion expressions) are derived as follows:

$$\mathbf{q}+\lambda_E\left(\frac{\partial \mathbf{q}}{\partial t}+\mathbf{V}\cdot\nabla\mathbf{q}-\mathbf{q}\cdot\nabla\mathbf{V}+(\nabla\cdot\mathbf{V})\mathbf{q}\right)=-k\nabla T, \tag{4}$$

$$\mathbf{J}+\lambda_C\left(\frac{\partial \mathbf{J}}{\partial t}+\mathbf{V}\cdot\nabla\mathbf{J}-\mathbf{J}\cdot\nabla\mathbf{V}+(\nabla\cdot\mathbf{V})\mathbf{J}\right)=-D_B\nabla C, \tag{5}$$

where $\mathbf{q}$ and $\mathbf{J}$ stand for heat and mass fluxes respectively, k for thermal conductivity, D_B for Brownian diffusivity, λ_E and λ_C for relaxation time of heat and mass fluxes respectively. Classical Fourier's and Fick's laws are deduced by inserting $\lambda_E = \lambda_C = 0$ in Eqs. (4) and (5). By considering the incompressibility condition $(\nabla\cdot\mathbf{V}=0)$ and steady flow with $(\frac{\partial \mathbf{q}}{\partial t}=0)$ and $(\frac{\partial \mathbf{J}}{\partial t}=0)$, Eqs. (4) and (5) can be rewritten as

$$\mathbf{q}+\lambda_E(\mathbf{V}\cdot\nabla\mathbf{q}-\mathbf{q}\cdot\nabla\mathbf{V})=-k\nabla T, \tag{6}$$

$$\mathbf{J}+\lambda_C(\mathbf{V}\cdot\nabla\mathbf{J}-\mathbf{J}\cdot\nabla\mathbf{V})=-D_B\nabla C. \tag{7}$$

The three dimensional energy and concentration equations take the following forms [45]:

$$u\frac{\partial T}{\partial x}+v\frac{\partial T}{\partial y}+w\frac{\partial T}{\partial z}+\lambda_E\Phi_E=\alpha_m\left(\frac{\partial^2 T}{\partial z^2}\right)+\frac{(\rho c)_p}{(\rho c)_f}(D_B\left(\frac{\partial T}{\partial z}\frac{\partial C}{\partial z}\right)+\frac{D_T}{T_\infty}\left(\frac{\partial T}{\partial z}\right)^2), \tag{8}$$

$$u\frac{\partial C}{\partial x}+v\frac{\partial C}{\partial y}+w\frac{\partial C}{\partial z}+\lambda_C\Phi_C=D_B\left(\frac{\partial^2 C}{\partial z^2}\right)+\frac{D_T}{T_\infty}\left(\frac{\partial^2 T}{\partial z^2}\right). \tag{9}$$

Here one has the following prescribed conditions:

$$u=U_w(x)=ax,\ v=V_w(y)=by,\ w=0,\ T=T_w,\ C=C_w \mathrm{at}\, z=0, \tag{10}$$

$$u\to 0,\ v\to 0,\ T\to T_\infty,\ C\to C_\infty \text{ as } z\to\infty, \tag{11}$$

where

$$\begin{aligned}\Phi_E&=u^2\frac{\partial^2 T}{\partial x^2}+v^2\frac{\partial^2 T}{\partial y^2}+w^2\frac{\partial^2 T}{\partial z^2}+2uv\frac{\partial^2 T}{\partial x\partial y}\\&\quad+2vw\frac{\partial^2 T}{\partial y\partial z}+2uw\frac{\partial^2 T}{\partial x\partial z}+\left(u\frac{\partial u}{\partial x}+v\frac{\partial u}{\partial y}+w\frac{\partial u}{\partial z}\right)\frac{\partial T}{\partial x}\\&\quad+\left(u\frac{\partial v}{\partial x}+v\frac{\partial v}{\partial y}+w\frac{\partial v}{\partial z}\right)\frac{\partial T}{\partial y}+(u\frac{\partial w}{\partial x}+v\frac{\partial w}{\partial y}+w\frac{\partial w}{\partial z})\frac{\partial T}{\partial z},\end{aligned} \tag{12}$$

and

$$\Phi_C = u^2\frac{\partial^2 C}{\partial x^2} + v^2\frac{\partial^2 C}{\partial y^2} + w^2\frac{\partial^2 C}{\partial z^2} + 2uv\frac{\partial^2 C}{\partial x\partial y} + 2vw\frac{\partial^2 C}{\partial y\partial z} + 2uw\frac{\partial^2 C}{\partial x\partial z} + \left(u\frac{\partial u}{\partial x} + v\frac{\partial u}{\partial y} + w\frac{\partial u}{\partial z}\right)\frac{\partial C}{\partial x} + \left(u\frac{\partial v}{\partial x} + v\frac{\partial v}{\partial y} + w\frac{\partial v}{\partial z}\right)\frac{\partial C}{\partial y} + \left(u\frac{\partial w}{\partial x} + v\frac{\partial w}{\partial y} + w\frac{\partial w}{\partial z}\right)\frac{\partial C}{\partial z}, \quad (13)$$

in which $\alpha_m = k/(\rho c)_f$, $(\rho c)_f$ and $(\rho c)_p$ stand for thermal diffusivity, heat capacity of liquid and effective heat capacity of nanoparticles respectively, D_B for Brownian diffusivity, T for temperature, C for concentration, D_T for thermophoretic diffusion coefficient, T_w and C_w for constant surface temperature and concentration respectively and T_∞ and C_∞ represent the ambient fluid temperature and concentration respectively. Selecting

$$\left.\begin{aligned} &u = axf'(\zeta), v = ayg'(\zeta), w = -(av)^{1/2}(f(\zeta)+g(\zeta)),\\ &\theta(\zeta) = \tfrac{T-T_\infty}{T_w-T_\infty}, \phi(\zeta) = \tfrac{C-C_\infty}{C_w-C_\infty}, \zeta = \left(\tfrac{a}{v}\right)^{1/2}z. \end{aligned}\right. \quad (14)$$

Eq. (1) is identically verified and Eqs. (2), (3) and (8)–(13) have been reduced to

$$f''' + (f+g)f'' - f'^2 = 0, \quad (15)$$

$$g''' + (f+g)g'' - g'^2 = 0, \quad (16)$$

$$\frac{1}{\Pr}\theta'' + N_b\theta'\phi' + N_t\theta'^2 + (f+g)\theta' - \delta_t((f+g)(f'+g')\theta' + (f+g)^2\theta'') = 0, \quad (17)$$

$$\frac{1}{Sc}\phi'' + \frac{N_t}{N_b}\frac{1}{Sc}\theta'' + (f+g)\phi' - \delta_c((f+g)(f'+g')\phi' + (f+g)^2\phi'') = 0, \quad (18)$$

$$f(0) = g(0) = 0,\ f'(0) = 1,\ g'(0) = \alpha,\ \theta(0) = 1,\ \phi(0) = 1, \quad (19)$$

$$f'(\infty) \to 0,\ g'(\infty) \to 0,\ \theta(\infty) \to 0,\ \phi(\infty) \to 0, \quad (20)$$

where (α) stands for ratio parameter, (Pr) shows Prandtl number, (N_b) depicts Brownian motion parameter, (N_t) gives thermophoresis parameter, (δ_t) denotes the nondimensional thermal relaxation parameter, (Sc) stands for Schmidt number and (δ_c) represents the nondimensional concentration relaxation parameter. These parameters can be specified by using the definitions given below:

$$\left.\begin{aligned} &\alpha = \tfrac{b}{a}, \Pr = \tfrac{v}{\alpha_m}, \delta_t = a\lambda_E, \delta_c = a\lambda_C,\\ &N_b = \tfrac{(\rho c)_p D_B (C_w - C_\infty)}{(\rho c)_f v}, N_t = \tfrac{(\rho c)_p D_T (T_w - T_\infty)}{(\rho c)_f v T_\infty}, Sc = \tfrac{v}{D_B}. \end{aligned}\right\} \quad (21)$$

Dimensionless expressions of skin-friction coefficients are as follows:

$$\left.\begin{aligned} &\mathrm{Re}_x^{1/2} C_{fx} = -f''(0),\\ &\mathrm{Re}_y^{1/2} C_{fy} = -\alpha^{-3/2} g''(0), \end{aligned}\right\} \quad (22)$$

where $\mathrm{Re}_x = U_w x/v$ and $\mathrm{Re}_y = V_w y/v$ depict the local Reynolds numbers.

3. Solutions by OHAM

Our purpose here is to develop the convergent homotopic solutions through the optimal homotopy analysis method (OHAM). Suitable initial approximations and the auxiliary linear operators for homotopic solutions are given by

$$\left.\begin{aligned} &f_0(\zeta) = 1 - \exp(-\zeta), g_0(\zeta) = \alpha(1 - \exp(-\zeta)),\\ &\theta_0(\zeta) = \exp(-\zeta), \phi_0(\zeta) = \exp(-\zeta), \end{aligned}\right\} \quad (23)$$

$$\left.\begin{aligned} &\mathcal{L}_f = \tfrac{d^3 f}{d\zeta^3} - \tfrac{df}{d\zeta}, \mathcal{L}_g = \tfrac{d^3 g}{d\zeta^3} - \tfrac{dg}{d\zeta},\\ &\mathcal{L}_\theta = \tfrac{d^2\theta}{d\zeta^2} - \theta, \mathcal{L}_\phi = \tfrac{d^2\phi}{d\zeta^2} - \phi. \end{aligned}\right\} \quad (24)$$

The above linear operators satisfy the following characteristics

$$\left.\begin{aligned} &\mathcal{L}_f[A_1^* + A_2^*\exp(\zeta) + A_3^*\exp(-\zeta)] = 0,\\ &\mathcal{L}_g[A_4^* + A_5^*\exp(\zeta) + A_6^*\exp(-\zeta)] = 0,\\ &\mathcal{L}_\theta[A_7^*\exp(\zeta) + A_8^*\exp(-\zeta)] = 0,\\ &\mathcal{L}_\phi[A_9^*\exp(\zeta) + A_{10}^*\exp(-\zeta)] = 0, \end{aligned}\right\} \quad (25)$$

in which A_j^* $(j = 1-10)$ stand for arbitrary constants.

4. Optimal convergence control parameters

Note that the non-zero convergence control parameters $\hbar_f, \hbar_g, \hbar_\theta$ and $\hbar_\phi$ in approximate homotopic solutions regulate the convergence zone and also rate of homotopic solutions. To obtain the optimal values of $\hbar_f, \hbar_g, \hbar_\theta$ and $\hbar_\phi$, we have employed the idea of minimization by representing the average squared residual errors as suggested by Liao [51].

$$\varepsilon_m^f = \frac{1}{k+1}\sum_{j=0}^{k}\left[\mathcal{N}_f\left(\sum_{i=0}^{m}\hat{f}(\zeta), \sum_{i=0}^{m}\hat{g}(\zeta)\right)_{\zeta=j\delta\zeta}\right]^2, \quad (26)$$

$$\varepsilon_m^g = \frac{1}{k+1}\sum_{j=0}^{k}\left[\mathcal{N}_g\left(\sum_{i=0}^{m}\hat{f}(\zeta), \sum_{i=0}^{m}\hat{g}(\zeta)\right)_{\zeta=j\delta\zeta}\right]^2, \quad (27)$$

$$\varepsilon_m^\theta = \frac{1}{k+1}\sum_{j=0}^{k}\left[\mathcal{N}_\theta\left(\sum_{i=0}^{m}\hat{f}(\zeta), \sum_{i=0}^{m}\hat{g}(\zeta), \sum_{i=0}^{m}\hat{\theta}(\zeta), \sum_{i=0}^{m}\hat{\phi}(\zeta),\right)_{\zeta=j\delta\zeta}\right]^2, \quad (28)$$

$$\varepsilon_m^\phi = \frac{1}{k+1}\sum_{j=0}^{k}\left[\mathcal{N}_\phi\left(\sum_{i=0}^{m}\hat{f}(\zeta), \sum_{i=0}^{m}\hat{g}(\zeta), \sum_{i=0}^{m}\hat{\theta}(\zeta), \sum_{i=0}^{m}\hat{\phi}(\zeta),\right)_{\zeta=j\delta\zeta}\right]^2. \quad (29)$$

Following Liao [51]

$$\varepsilon_m^t = \varepsilon_m^f + \varepsilon_m^g + \varepsilon_m^\theta + \varepsilon_m^\phi, \quad (30)$$

where ε_m^t stands for total squared residual error, $k = 20$ and $\delta\zeta = 0.5$. The total average squared residual error is minimized by employing Mathematica package BVPh2.0. A case has been considered where $\alpha = N_t = 0.1, N_b = 0.3, \delta_t = \delta_c = 0.2$ and $\Pr = Sc = 1.0$. The optimal values of convergence-control parameters at 2nd order of approximations are $\hbar_f = -1.64104, \hbar_g = -1.02624$, $\hbar_\theta = -0.933309$ and $\hbar_\phi = -0.946239$ and the total averaged squared residual error is $\varepsilon_m^t = 2.61 \times 10^{-4}$. Table 1 shows the individual average squared residual error employing the optimal values of convergence control parameters at $m = 2$. It is observed that the averaged squared residual error reduces with higher order approximations.

5. Discussion

This portion explores the impacts of various pertinent parameters like ratio parameter (α), Prandtl number (Pr), Schmidt number (Sc), Brownian motion parameter (N_b), thermophoresis parameter (N_t), thermal relaxation parameter (δ_t) and concentration relaxation parameter (δ_c) on temperature $\theta(\zeta)$ and concentration $\phi(\zeta)$ distributions. Fig. 1 presents that the larger values of ratio param-

Table 1
Individual averaged squared residual errors considering optimal values of auxiliary parameters.

m	ε_m^f	ε_m^g	ε_m^θ	ε_m^ϕ
2	4.27×10^{-6}	1.29×10^{-7}	1.40×10^{-4}	1.17×10^{-4}
6	4.47×10^{-8}	1.35×10^{-10}	4.69×10^{-7}	1.11×10^{-6}
10	7.13×10^{-10}	3.77×10^{-13}	4.43×10^{-9}	7.21×10^{-8}
16	1.83×10^{-12}	6.35×10^{-16}	4.41×10^{-11}	9.87×10^{-10}
20	3.73×10^{-14}	1.63×10^{-17}	4.75×10^{-12}	7.80×10^{-11}
26	1.18×10^{-16}	5.18×10^{-20}	6.96×10^{-14}	1.41×10^{-12}
30	2.62×10^{-18}	1.20×10^{-21}	3.47×10^{-15}	9.38×10^{-14}

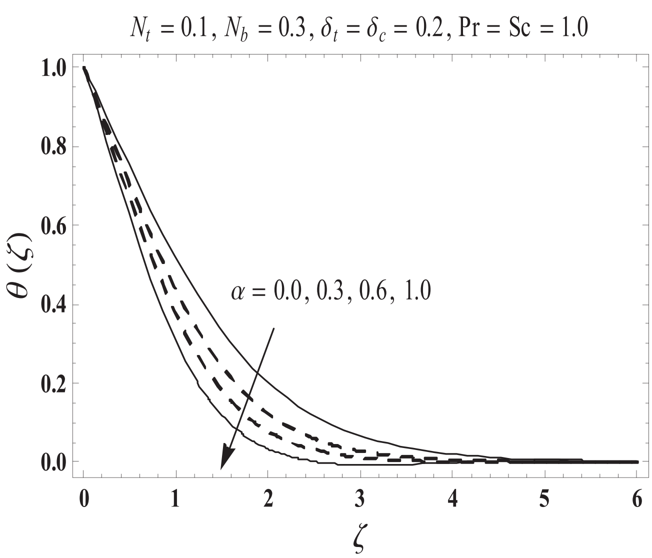

Fig. 1. Effect of α on $\theta(\zeta)$.

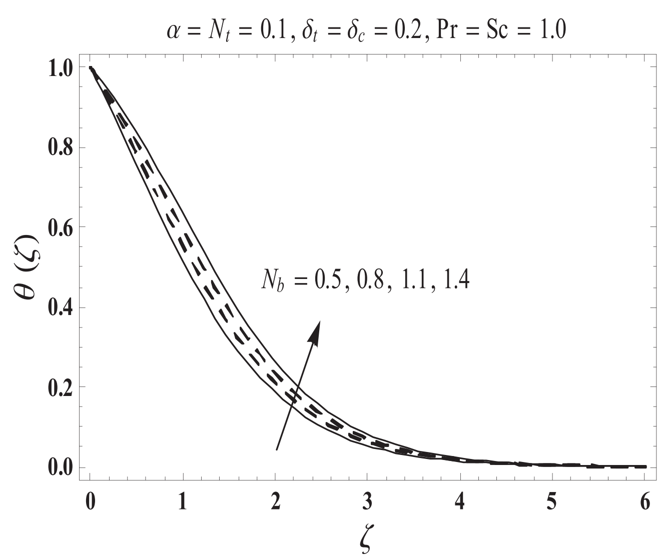

Fig. 3. Effect of N_b on $\theta(\zeta)$.

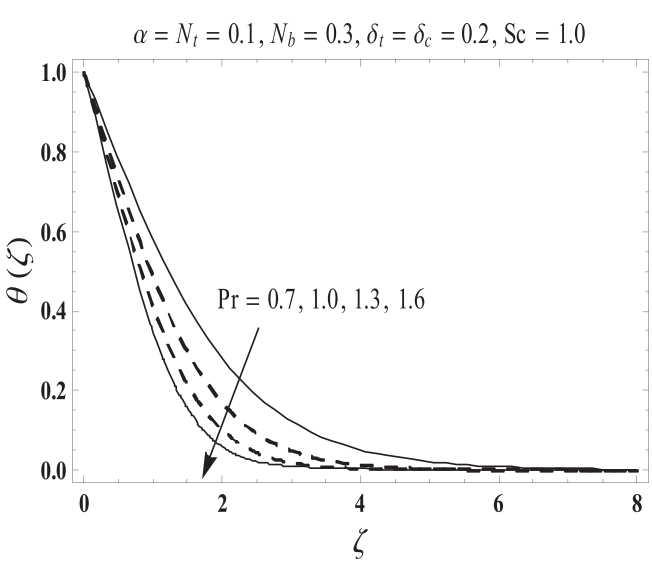

Fig. 2. Effect of Pr on $\theta(\zeta)$.

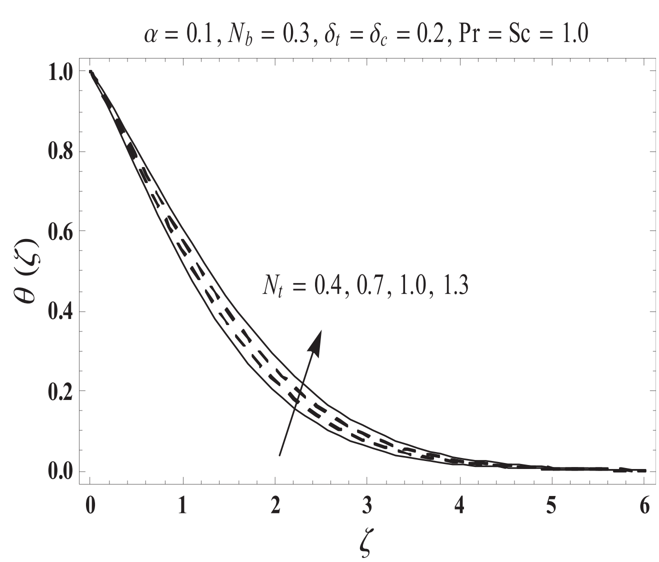

Fig. 4. Effect of N_t on $\theta(\zeta)$.

eter (α) lead to lower temperature $\theta(\zeta)$ and less thermal layer. Further two-dimensional (2D) flow case is obtained when $\alpha = 0$. Fig. 2 demonstrates that how the temperature field $\theta(\zeta)$ is get effected by Prandtl number (Pr). It is observed that by enhancing Prandtl number (Pr), the temperature field $\theta(\zeta)$ and thermal layer thickness reduces. Physically, as Prandtl number (Pr) is an integral part of thermal diffusivity, therefore, thermal diffusivity is responsible for lower temperature. Greater values of Prandtl number (Pr) yields weaker thermal diffusivity which corresponds to lower temperature field and less thickness of thermal layer. Fig. 3 shows the variation in temperature field $\theta(\zeta)$ for distinct values of Brownian motion parameter (N_b). It has been clearly noted that by increasing Brownian motion parameter (N_b), an enhancement appeared in temperature field $\theta(\zeta)$ and its related thermal layer thickness.

Fig. 4 is drawn to depict the influence of thermophoreis parameter (N_t) on temperature field $\theta(\zeta)$. Increasing values of thermophoresis parameter (N_t) constitutes a higher temperature field and thermal layer thickness. The reason behind this argument is that an enhancement in (N_t) yields a stronger thermophoretic force which allows deeper migration of nanoparticles in the fluid which is far away from the surface forms a higher temperature field and thickness of thermal layer. Fig. 5 presents variation in the temperature field $\theta(\zeta)$ for different values of thermal relaxation parameter (δ_t). It has been clearly examined that an enhancement in the value of thermal relaxation parameter (δ_t) shows decreasing behavior for temperature field $\theta(\zeta)$ and thermal layer thickness. Here $(\delta_t = 0)$ represents that the present model is reduced to classical Fourier's law. Fig. 6 depicts that increasing values of ratio parameter (α) presents a weaker concentration distribution $\phi(\eta)$ and associated less thickness of concentration layer. Fig. 7 presents that the greater Schmidt number (Sc) forms a reduction in the concentration field $\phi(\zeta)$. Physically Schmidt number is based on Brownian diffusivity. An increase in Schmidt number (Sc) yields weaker Brownian diffusivity. Such weaker Brownian diffusivity corresponds to lower concentration field $\phi(\zeta)$. From Fig. 8, it is clearly examined that a weaker concentration field $\phi(\zeta)$ is generated by using larger Brownian motion parameter (N_b). Fig. 9 shows that the higher thermophoresis parameter (N_t) produce a stronger concentration field $\phi(\zeta)$. Fig. 10 presents how concentration relaxation parameter (δ_c) effects concentration field $\phi(\zeta)$. By increasing (δ_c), both concentration $\phi(\zeta)$ and thickness of concentration layer decreases. Here $(\delta_c = 0)$ represents that the present model is reduced to classical Fick's law. Table 2 is developed to analyze the coefficients of skin-friction $-\mathrm{Re}_x^{1/2}C_{fx}$ and $-\mathrm{Re}_y^{1/2}C_{fy}$ for several values of α. It is seen that the coefficients of skin-friction show opposite behavior for larger ratio parameter (α). Table 3 is calculated in order to investigate the numerical computations of heat transfer rate $-\theta'(0)$ for distinct values of thermal relaxation parameter (δ_t). Here we examined that the heat transfer rate has higher values by incrementing (δ_t). Table 4 depicts the numerical values of mass transfer rate $-\phi'(0)$ for distinct values of concentration relaxation parameter (δ_c). Here we observed that the values of

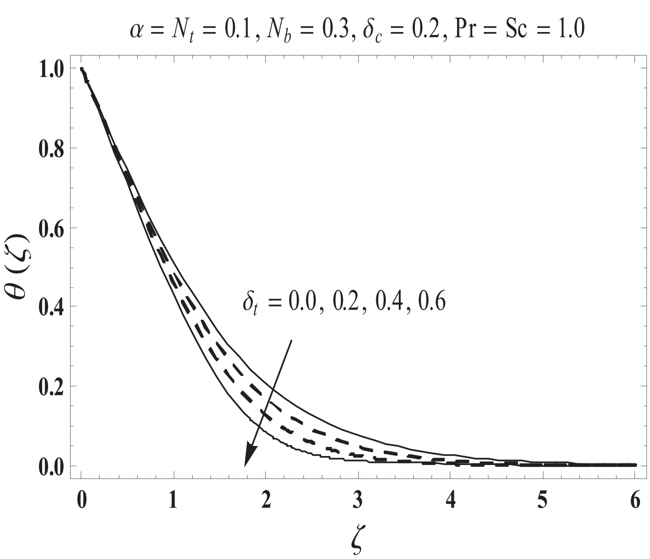

Fig. 5. Effect of δ_t on $\theta(\zeta)$.

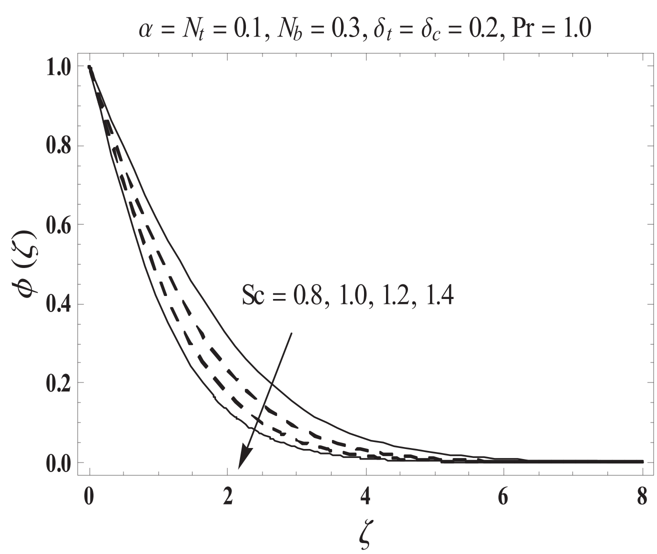

Fig. 7. Effect of Sc on $\phi(\zeta)$.

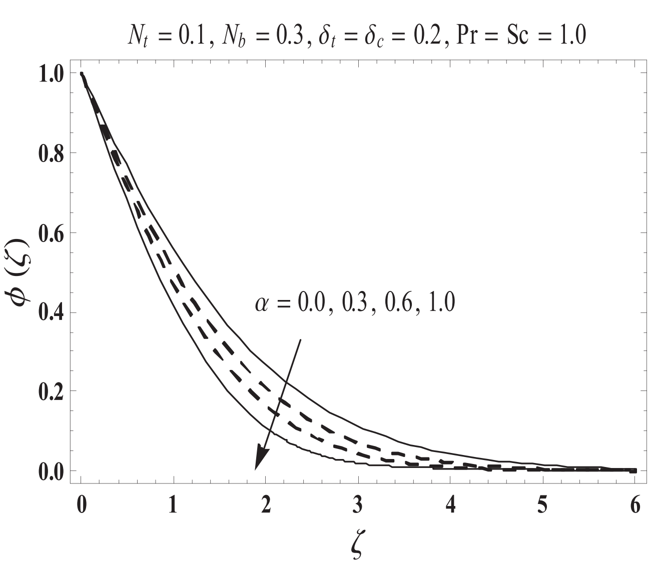

Fig. 6. Effect of α on $\phi(\zeta)$.

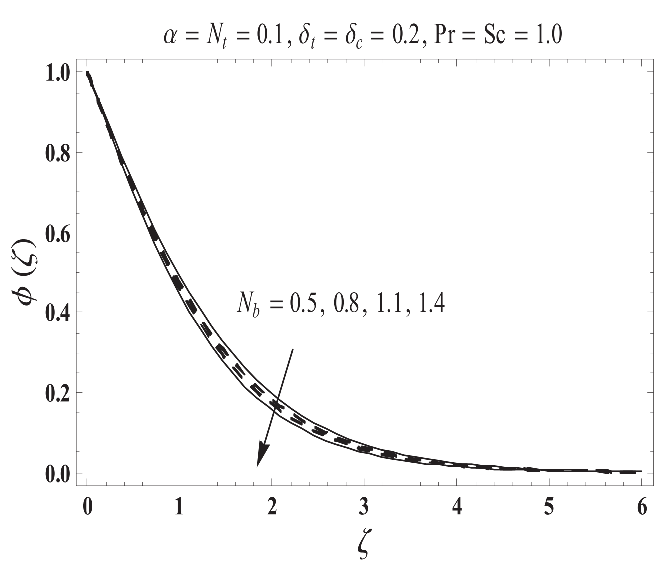

Fig. 8. Effect of N_b on $\phi(\zeta)$.

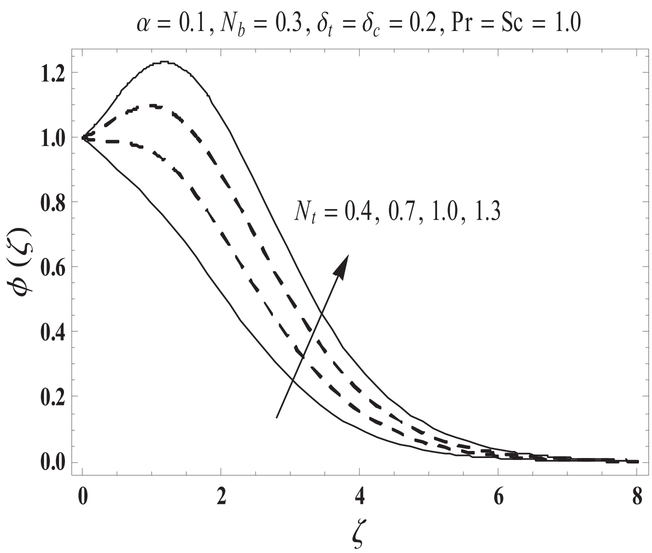

Fig. 9. Effect of N_t on $\phi(\zeta)$.

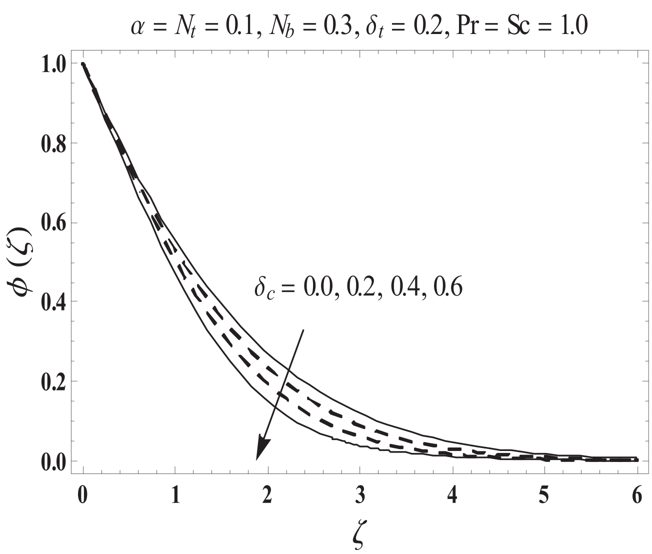

Fig. 10. Effect of δ_c on $\phi(\zeta)$.

Table 2
Numerical data for coefficients of skin-friction $-\mathrm{Re}_x^{1/2}C_{fx}$ and $-\mathrm{Re}_y^{1/2}C_{fy}$ for several values of α.

α	0.1	0.4	0.7	1.0
$-\mathrm{Re}_x^{1/2}C_{fx}$	1.02026	1.07579	1.12640	1.17372
$-\mathrm{Re}_y^{1/2}C_{fy}$	2.11389	1.38037	1.23711	1.17372

Table 3
Numerical values of heat transfer rate $-\theta'(0)$ for different values of δ_t when $\alpha = N_t = 0.1, N_b = 0.3, \delta_c = 0.2$ and $\Pr = Sc = 1.0$.

δ_t	0.0	0.1	0.2	0.3
$-\theta'(0)$	0.51107	0.51884	0.52697	0.53541

Table 4
Numerical values of mass transfer rate $-\phi'(0)$ for different values of δ_c when $\alpha = N_t = 0.1, N_b = 0.3, \delta_t = 0.2$ and $\Pr = Sc = 1.0$.

δ_c	0.0	0.1	0.2	0.3
$-\phi'(0)$	0.50540	0.51536	0.52574	0.53673

mass transfer rate are greater when larger values of (δ_c) are considered.

6. Conclusions

Three dimensional (3D) boundary-layer flow of viscous nanofluid by a linear stretching surface with Cattaneo–Christov double diffusion expressions of heat and mass transfer has been examined. The key points of presented analysis are listed below:

- Increasing values of ratio parameter (α) depict decreasing behavior for temperature $\theta(\zeta)$ and concentration $\phi(\zeta)$.
- An increment in Prandtl number $(\Pr)$ shows decreasing trend in temperature $\theta(\zeta)$ and thermal layer thickness.
- Both temperature $\theta(\zeta)$ and concentration $\phi(\zeta)$ fields show opposite behavior for larger Brownian motion parameter (N_b).
- By increasing the thermophoresis parameter (N_t), an enhancement is observed in both temperature $\theta(\zeta)$ and concentration $\phi(\zeta)$ fields.
- Both temperature field $\theta(\zeta)$ and its associated thermal layer thickness decrease by increasing thermal relaxation parameter (δ_t).
- Higher concentration relaxation parameter (δ_c) causes a decay in the concentration field $\phi(\zeta)$.
- Skin friction coefficients show opposite trend for increasing values of ratio parameter (α).
- Both heat and mass transfer rates at the surface are higher for larger thermal (δ_t) and concentration (δ_c) relaxation parameters.

References

[1] Sakiadis BC. Boundary-layer behaviour on continuous solid surfaces: II. The boundary layer on a continuous flat surface. AIChE J. 1961;7:221–5.
[2] Crane LJ. Flow past a stretching plate. Z. Angew. Math. Phys. 1970;21:645–7.
[3] Wang CY. The three-dimensional flow due to a stretching flat surface. Phys. Fluids 1984;27:1915–7.
[4] Ariel PD. The three-dimensional flow past a stretching sheet and the homotopy perturbation method. Comput. Math. Appl. 2007;54:920–5.
[5] Xu H, Liao SJ, Pop I. Series solutions of unsteady three-dimensional MHD flow and heat transfer in the boundary layer over an impulsively stretching plate. Eur. J. Mech. B/Fluids 2007;26:15–27.
[6] Hayat T, Qasim M, Abbas Z. Homotopy solution for the unsteady three-dimensional MHD flow and mass transfer in a porous space. Commun. Nonlinear Sci. Numer. Simul. 2010;15:2375–87.
[7] Liu IC, Wang HH, Peng YF. Flow and heat transfer for three-dimensional flow over an exponentially stretching surface. Chem. Eng. Commun. 2013;200:253–68.
[8] Hayat T, Muhammad T, Shehzad SA, Alsaedi A. Soret and Dufour effects in three-dimensional flow over an exponentially stretching surface with porous medium, chemical reaction and heat source/sink. Int. J. Numer. Methods Heat Fluid Flow 2015;25:762–81.
[9] J.B.J. Fourier, Théorie Analytique De La Chaleur, Paris, 1822.
[10] Cattaneo C. Sulla conduzione del calore. Atti Semin. Mat. Fis. Univ. Modena Reggio Emilia 1948;3:83–101.
[11] Christov CI. On frame indifferent formulation of the Maxwell-Cattaneo model of finite-speed heat conduction. Mech. Res. Commun. 2009;36:481–6.
[12] Straughan B. Thermal convection with the Cattaneo-Christov model. Int. J. Heat Mass Transfer 2010;53:95–8.
[13] Ciarletta M, Straughan B. Uniqueness and structural stability for the Cattaneo-Christov equations. Mech. Res. Commun. 2010;37:445–7.
[14] Haddad SAM. Thermal instability in Brinkman porous media with Cattaneo-Christov heat flux. Int. J. Heat Mass Transfer 2014;68:659–68.
[15] Han S, Zheng L, Li C, Zhang X. Coupled flow and heat transfer in viscoelastic fluid with Cattaneo-Christov heat flux model. Appl. Math. Lett. 2014;38:87–93.
[16] Mustafa M. Cattaneo-Christov heat flux model for rotating flow and heat transfer of upper-convected Maxwell fluid. AIP Adv. 2015;5:047109.
[17] Khan JA, Mustafa M, Hayat T, Alsaedi A. Numerical study of Cattaneo-Christov heat flux model for viscoelastic flow due to an exponentially stretching surface. Plos One 2015;10:e0137363.
[18] Hayat T, Muhammad T, Alsaedi A, Mustafa M. A comparative study for flow of viscoelastic fluids with Cattaneo-Christov heat flux. Plos One 2016;11: e0155185.

[19] Li J, Zheng L, Liu L. MHD viscoelastic flow and heat transfer over a vertical stretching sheet with Cattaneo-Christov heat flux effects. J. Mol. Liq. 2016;221:19–25.
[20] Mushtaq A, Abbasbandy S, Mustafa M, Hayat T, Alsaedi A. Numerical solution for Sakiadis flow of upper-convected Maxwell fluid using Cattaneo-Christov heat flux model. AIP Adv. 2016;6:015208.
[21] Shehzad SA, Abbasi FM, Hayat T, Alsaedi A. Cattaneo-Christov heat flux model for Darcy-Forchheimer flow of an Oldroyd-B fluid with variable conductivity and non-linear convection. J. Mol. Liq. 2016;224:274–8.
[22] Hayat T, Imtiaz M, Alsaedi A, Almezal S. On Cattaneo-Christov heat flux in MHD flow of Oldroyd-B fluid with homogeneous-heterogeneous reactions. J. Magn. Magn. Mater. 2016;401:296–303.
[23] S.U.S. Choi, Enhancing thermal conductivity of fluids with nanoparticles, USA, ASME, FED 231/MD, 66 (1995) 99–105.
[24] Buongiorno J. Convective transport in nanofluids. ASME J. Heat Transfer 2006;128:240–50.
[25] Makinde OD, Aziz A. Boundary layer flow of a nanofluid past a stretching sheet with a convective boundary condition. Int. J. Thermal Sci. 2011;50:1326–32.
[26] Mustafa M, Hayat T, Pop I, Asghar S, Obaidat S. Stagnation-point flow of a nanofluid towards a stretching sheet. Int. J. Heat Mass Transfer 2011;54:5588–94.
[27] Turkyilmazoglu M. Exact analytical solutions for heat and mass transfer of MHD slip flow in nanofluids. Chem. Eng. Sci. 2012;84:182–7.
[28] Ibrahim W, Makinde OD. The effect of double stratification on boundary layer flow and heat transfer of nanofluid over a vertical plate. Comput. Fluids 2013;86:433–41.
[29] Sheikholeslami M, Bandpy MG, Ellahi R, Hassan M, Soleimani S. Effects of MHD on Cu-water nanofluid flow and heat transfer by means of CVFEM. J. Magn. Magn. Mater. 2014;349:188–200.
[30] Hayat T, Muhammad T, Shehzad SA, Alsaedi A. A mathematical study for three-dimensional boundary layer flow of Jeffrey nanofluid. Z. Naturforsch. A 2015;70a:225–33.
[31] Goodarzi M, Safaei MR, Vafai K, Ahmadi G, Dahari M, Kazi SN, Jomhari N. Investigation of nanofluid mixed convection in a shallow cavity using a two-phase mixture model. Int. J. Thermal Sci. 2014;75:204–20.
[32] Hayat T, Aziz A, Muhammad T, Ahmad B. Influence of magnetic field in three dimensional flow of couple stress nanofluid over a nonlinearly stretching surface with convective condition. Plos One 2015;10:e0145332.
[33] Malvandi A, Safaei MR, Kaffash MH, Ganji DD. MHD mixed convection in a vertical annulus filled with Al_2O_3–water nanofluid considering nanoparticle migration. J. Magn. Magn. Mater. 2015;382:296–306.
[34] Hayat T, Muhammad T, Alsaedi A, Alhuthali MS. Magnetohydrodynamic three-dimensional flow of viscoelastic nanofluid in the presence of nonlinear thermal radiation. J. Magn. Magn. Mater. 2015;385:222–9.
[35] Chamkha A, Abbasbandy S, Rashad AM. Non-Darcy natural convection flow for non-Newtonian nanofluid over cone saturated in porous medium with uniform heat and volume fraction fluxes. Int. J. Numer. Methods Heat Fluid Flow 2015;25:422–37.
[36] Gireesha BJ, Gorla RSR, Mahanthesh B. Effect of suspended nanoparticles on three-dimensional MHD flow, heat and mass transfer of radiating Eyring-Powell fluid over a stretching sheet. J. Nanofluids 2015;4:474–84.
[37] Hayat T, Imtiaz M, Alsaedi A. Impact of magnetohydrodynamics in bidirectional flow of nanofluid subject to second order slip velocity and homogeneous-heterogeneous reactions. J. Magn. Magn. Mater. 2015;395:294–302.
[38] Ellahi R, Hassan M, Zeeshan A. Shape effects of nanosize particles in Cu-H_2O nanofluid on entropy generation. Int. J. Heat Mass Transfer 2015;81:449–56.
[39] Sheikholeslami M, Ellahi R. Three dimensional mesoscopic simulation of magnetic field effect on natural convection of nanofluid. Int. J. Heat Mass Transfer 2015;89:799–808.
[40] Sheikholeslami M, Ellahi R. Electrohydrodynamic nanofluid hydrothermal treatment in an enclosure with sinusoidal upper wall. Appl. Sci. 2015;5:294–306.
[41] Hayat T, Muhammad T, Qayyum A, Alsaedi A, Mustafa M. On squeezing flow of nanofluid in the presence of magnetic field effects. J. Mol. Liq. 2016;213:179–85.
[42] Hsiao KL. Stagnation electrical MHD nanofluid mixed convection with slip boundary on a stretching sheet. Appl. Thermal Eng. 2016;98:850–61.
[43] Hayat T, Muhammad T, Shehzad SA, Alsaedi A. On three-dimensional boundary layer flow of Sisko nanofluid with magnetic field effects. Adv. Powder Tech. 2016;27:504–12.
[44] Malvandi A, Ganji DD, Pop I. Laminar filmwise condensation of nanofluids over a vertical plate considering nanoparticles migration. Appl. Thermal Eng. 2016;100:979–86.
[45] Sui J, Zheng L, Zhang X. Boundary layer heat and mass transfer with Cattaneo-Christov double-diffusion in upper-convected Maxwell nanofluid past a stretching sheet with slip velocity. Int. J. Thermal Sci. 2016;104:461–8.
[46] Hayat T, Aziz A, Muhammad T, Alsaedi A. On magnetohydrodynamic three-dimensional flow of nanofluid over a convectively heated nonlinear stretching surface. Int. J. Heat Mass Transfer 2016;100:566–72.
[47] Rahman SU, Ellahi R, Nadeem S, Zia QMZ. Simultaneous effects of nanoparticles and slip on Jeffrey fluid through tapered artery with mild stenosis. J. Mol. Liq. 2016;218:484–93.
[48] Akbarzadeh M, Rashidi S, Bovand M, Ellahi R. A sensitivity analysis on thermal and pumping power for the flow of nanofluid inside a wavy channel. J. Mol. Liq. 2016;220:1–13.
[49] Hayat T, Waqas M, Khan MI, Alsaedi A. Analysis of thixotropic nanomaterial in a doubly stratified medium considering magnetic field effects. Int. J. Heat Mass Transfer 2016;102:1123–9.
[50] Hayat T, Hussain Z, Alsaedi A, Asghar S. Carbon nanotubes effects in the stagnation point flow towards a nonlinear stretching sheet with variable thickness. Adv. Powder Tech. 2016;27:1677–88.
[51] Liao SJ. An optimal homotopy-analysis approach for strongly nonlinear differential equations. Commun. Nonlinear Sci. Numer. Simul. 2010;15:2003–16.
[52] Dehghan M, Manafian J, Saadatmandi A. Solving nonlinear fractional partial differential equations using the homotopy analysis method. Numer. Meth. Partial Diff. Eq. 2010;26:448–79.
[53] Turkyilmazoglu M. Solution of the Thomas-Fermi equation with a convergent approach. Commun. Nonlinear Sci. Numer. Simul. 2012;17:4097–103.
[54] Malvandi A, Hedayati F, Domairry G. Stagnation point flow of a nanofluid toward an exponentially stretching sheet with nonuniform heat generation/absorption. J. Thermodynamics 2013;2013:764827.
[55] Abbasbandy S, Hashemi MS, Hashim I. On convergence of homotopy analysis method and its application to fractional integro-differential equations. Quaestiones Mathematicae 2013;36:93–105.
[56] Sui J, Zheng L, Zhang X, Chen G. Mixed convection heat transfer in power law fluids over a moving conveyor along an inclined plate. Int. J. Heat Mass Transfer 2015;85:1023–33.
[57] Zeeshan A, Majeed A, Ellahi R. Effect of magnetic dipole on viscous ferro-fluid past a stretching surface with thermal radiation. J. Mol. Liq. 2016;215:549–54.
[58] Hayat T, Hussain Z, Muhammad T, Alsaedi A. Effects of homogeneous and heterogeneous reactions in flow of nanofluids over a nonlinear stretching surface with variable surface thickness. J. Mol. Liq. 2016;221:1121–7.
[59] Hayat T, Abbas T, Ayub M, Farooq M, Alsaedi A. Flow of nanofluid due to convectively heated Riga plate with variable thickness. J. Mol. Liq. 2016;222:854–62.
[60] Hayat T, Muhammad T, Shehzad SA, Alsaedi A. An analytical solution for magnetohydrodynamic Oldroyd-B nanofluid flow induced by a stretching sheet with heat generation/absorption. Int. J. Thermal Sci. 2017;111:274–88.